ACS APPLIED MATERIALS & INTERFACES

Research Article

www.acsami.org

Gate-Voltage-Controlled Spin and Valley Polarization Transport in a Normal/Ferromagnetic/Normal MoS_2 Junction

Hai Li, Jianmei Shao, Daoxin Yao, and Guowei Yang*

State Key Laboratory of Optoelectronic Materials and Technologies, Institute of Optoelectronic and Functional Composite Materials, Nanotechnology Research Center, School of Physics and Engineering, Sun Yat-sen University, Guangzhou 510275, Guangdong, People's Republic of China

ABSTRACT: Two-dimensional (2D) materials are extensively explored due to the remarkable physical property and the great potential for post-silicon electronics since the landmark achievement of graphene. The monolayer (ML) MoS_2 with a direct energy gap is a typical 2D material and promising candidate for a wide range of device applications. The extensive efforts so far have focused on the optical valley control applications of ML MoS_2 rather than the electrical control of spin and valley transport. However, the electrical manipulation of spin injection and transport is essential to realize practical spintronics applications. Here, we theoretically demonstrated that the valley and spin transport can be electrically manipulated by a gate voltage in a normal/ferromagnetic/normal monolayer MoS_2 junction device. It was found that the *fully* valley- and spin-polarized conductance can be achieved due to the spin−valley coupling of valence-band edges together with the exchange field, and both the amplitude and direction of the *fully* spin-polarized conductance can be modulated by the gate voltage. These findings not only provided deep understanding to the basic physics in the spin and valley transport of ML MoS_2 but also opened an avenue for the electrical control of valley and spin transport in monolayer dichalcogenide-based devices.

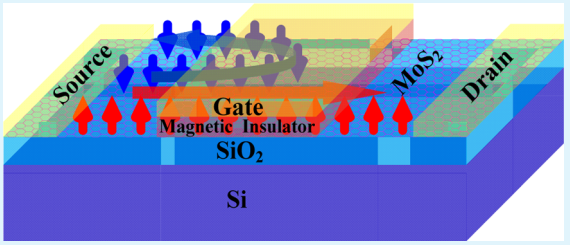

KEYWORDS: *spintronics, valleytronics, MoS_2, spin, valley, polarization*

INTRODUCTION

Owing to the remarkable physical properties and the great potential for post-silicon electronics, two-dimensional (2D) materials[1−9] have been extensively explored since the landmark achievement of graphene.[1−3] Recently, some significant developments have demonstrated that the monolayer (ML) MoS_2,[6−9] a typical layered transition-metal dichalcogenide, is a semiconductor with a relatively large direct energy gap (∼1.8 eV).[10−13] It is demonstrated that ML MoS_2 has reasonable in-plane carrier mobility, high thermal stability, and good compatibility with standard semiconductor manufacturing.[14] These satisfied properties render ML MoS_2 as a promising candidate for a wide range of applications, including photoluminescence at visible wavelengths,[10,15] photodetectors with high responsivity,[12] and field-effect transistors[14,16,17] with room-temperature current on/off ratios exceeding 10^8. Unlike graphene, where the spin−orbit coupling (SOC) vanishes,[18,19] ML MoS_2 has strong SOC, and this characteristic together with the inversion asymmetry gives rise to large valley-dependent spin splitting on the top of valence bands.[7−9,11,20−22] It is noteworthy that the exotic spin splitting can suppress the spin relaxation and result in long spin lifetimes regardless of the strong SOC.[7,21−24] Recent polarization-resolved photoluminescence measurements have observed that the spin lifetimes in ML MoS_2 can reach to the order of 1 ns,[23] which opens a realm of spintronics applications in ML MoS_2-based devices. In addition, the conduction and valence-band edges of ML MoS_2 constitute a binary index for low-energy carriers. Due to the large valley separation in the momentum space, the valley index is robust against smooth deformation and low-energy phonons.[7] This characteristic can be interesting to explore potential applications in valleytronics.[23−25] Indeed, some precursory works have demonstrated the viability of the valley-based electronic[24,25] and optical valley control applications of ML MoS_2.[23]

In contrast to the extensive theoretical and experimental efforts on the photoluminescence, transistors, and optical valley control applications of ML MoS_2, the electrical control of spin and valley transport in ML MoS_2 has not been explored yet. As a major goal of spintronics, the electrical manipulation of spin injection and transport is essential to realize practical spintronics applications. In light of the above discussion, in this contribution, we theoretically propose a normal/ferromagnetic/normal (NFN) monolayer MoS_2 junction and investigate the gate-voltage-tuned charge and valley and spin transport properties. Intriguingly, we find that the *fully* valley- and spin-polarized currents can be obtained simultaneously in this device. We emphasize that the spin splitting near the valence-band edges is essential to the valley-polarized transport, and this characteristic can only exist in ML MoS_2 but is absent in graphene[26,27] and silicene.[28] Importantly, both the amplitude and direction of the spin-polarized currents can be conveniently

Received: October 27, 2013
Accepted: January 8, 2014
Published: January 13, 2014

   dx.doi.org/10.1021/am4047602 | *ACS Appl. Mater. Interfaces* 2014, 6, 1759−1764

modulated by the gate voltage. Additionally, the conditions for realizing the *fully* valley- and spin-polarized conductance are deduced analytically. These results thus introduce the transition-metal dichalcogenide as a fascinating material for spin- and valleytronics and open up an avenue for the electrical control of valley and spin polarization transport in ML MoS_2.

THEORY

We consider a NFN junction based on the monolayer MoS_2, as shown in Figure 1. A voltage gate is placed on the top of the

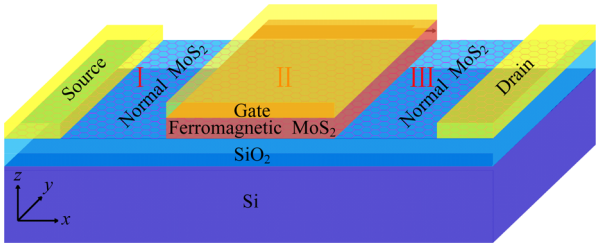

Figure 1. Illustration of normal/ferromagnetic/normal monolayer MoS_2 junction device.

ferromagnetic region to generate an electrostatic modulation, and the electrostatic potential is taken as U in the ferromagnetic region and 0 otherwise. We emphasize here that, in stark contrast to that of ref 28, the electrostatic potential in the proposed model is only utilized to tune the Fermi level but not to modulate the energy gap as well as the topological phase. Actually, for a flat ML MoS_2 sheet, the energy gap cannot be modulated by a perpendicular electric field.[29−31] The exchange field can be induced by the magnetic proximity effect, which has been extensively explored in graphene,[26,27] silicene,[28] and conventional two-dimensional electron gas.[32] As proposed by Ye et al.,[32] by depositing an array of ferromagnetic dysprosium strips on the top of a GaAs−AlGaAs heterojunction, a considerable one-dimensional periodic magnetic field can be achieved. Similar method can be used in our device to get an exchanged field.

Here we assume the strip width L_y (along the y direction) is much larger than the strip length L (along the x direction), so that the microscopic details of the strip edges can be safely neglected and the translational invariance in the y direction is preserved. These assumptions have been extensively applied to similar models based on graphene[33−35] and TI.[36−38]

To linear order in k, the effective Hamiltonian in the ferromagnetic region is given by[7−9]

$$H = \hbar v(\tau_z k_x \sigma_x + k_y \sigma_y) + \Delta\sigma_z + (-\lambda\tau_z s_z \sigma_z + \lambda\tau_z s_z) - s_z h + U \quad (1)$$

where $\tau_z = \pm 1$ denotes the K and K′ valleys, respectively, while $s_z = \pm 1$ stands for the electron spin ↑and ↓, and the Pauli matrices $\sigma_{x,y,z}$ operate on the space of the d_{z^2} and $(d_{x^2-y^2} \pm id_{xy})/\sqrt{2}$ orbitals; $k_{x,y}$ is the momentum measured with respect to the K(K′) point, the Fermi velocity $v = 5.3 \times 10^5$ m·s^{-1}, λ = 37.5 meV is the spin splitting near the valence-band edges induced by the SOC, and Δ = 833 meV is the band gap originating from the inversion asymmetry between orbitals d_{z^2} and $(d_{x^2-y^2} \pm id_{xy})/\sqrt{2}$.[7−9] Here, h is the exchange field added in the ferromagnetic region. According to eq 1, the energy dispersions in the ferromagnetic region are given by

$$E_\pm = U + (\tau_z s_z \lambda - s_z h) \pm \sqrt{(\Delta - \tau_z s_z \lambda)^2 + (\hbar v k')^2} \quad (2)$$

where $k'^2 = (\tau_z k'_x)^2 + k_y^2$ and ± labels the occupied and empty bands, respectively. In the normal regions, the energy dispersions can be obtained by substituting $h = 0$, $U = 0$, and $k^2 = (\tau_z k_x)^2 + k_y^2$ into eq 2. It is important to point out that the effective continuum model described in eq 1 is only valid for the low-lying physics of ML MoS_2. Thus, the corresponding parameters should be chosen to ensure the validity of eq 1. Additionally, the responses of conduction bands and valence bands to the exchanged field should be different due to their different orbit originations. Nevertheless, we neglect this point in all calculations. This approximation is valid, as it has been successfully utilized in some literature.[8,9]

Owing to the translational invariance in the y direction, the wave function in each region can be described as

$$\Psi_{\mathrm{I}} = e^{ik_y y}\left\{\frac{1}{E_N}\begin{pmatrix}\hbar v k_-\\ E_M\end{pmatrix}e^{ik_x x} + \frac{r_{\tau_z s_z}}{E_N}\begin{pmatrix}-\hbar v k_+\\ E_M\end{pmatrix}e^{-ik_x x}\right\} \quad (3)$$

$$\Psi_{\mathrm{II}} = e^{ik_y y}\left\{a_{\tau_z s_z}\begin{pmatrix}\hbar v k'_-\\ E_F\end{pmatrix}e^{ik'_x x} + b_{\tau_z s_z}\begin{pmatrix}-\hbar v k'_+\\ E_F\end{pmatrix}e^{-ik'_x x}\right\} \quad (4)$$

$$\Psi_{\mathrm{III}} = \frac{t_{\tau_z s_z}}{E_N}\begin{pmatrix}\hbar v k_-\\ E_M\end{pmatrix}e^{i(k_x x + k_y y)} \quad (5)$$

with $k_\pm = \tau_z k_x \pm ik_y$, $k'_\pm = \tau_z k'_x \pm ik_y$, $E_M = E_\pm - \Delta$, $E_N = ((\hbar v k)^2 + E_M^2)^{1/2}$, and $E_F = E_\pm - U - \Delta + s_z h$, where $a_{\tau_z s_z}$, $b_{\tau_z s_z}$, $r_{\tau_z s_z}$, and $t_{\tau_z s_z}$ are the valley- and spin-resolved scattering coefficients. Then, following the standard procedure of mating the wave functions at the interfaces of regions I and II and regions II and III (see Figure 1), the spin- and valley-resolved transmission probability can be analytically obtained

$$T_{\tau_z s_z} = \left|\frac{4k_x k'_x E_M E_F e^{-ik_x L}}{\xi e^{ik'_x L}}\right|^2 \quad (6)$$

where $\xi = \{E_M^2 k'^2 + E_M E_F(k_+k'_+ + k_-k'_-) + E_F^2 k^2\}e^{-2ik_x' L} + E_M E_F(k_+k'_- + k_-k'_+) - E_M^2 k'^2 - E_F^2 k^2$. From the transmission probability, the normalized valley- and spin-resolved conductance at zero temperature is given by[28]

$$G_{\tau_z s_z} = \frac{1}{2}\int_{-\pi/2}^{\pi/2} T_{\tau_z s_z}\cos\theta\, \mathrm{d}\theta \quad (7)$$

where $\theta = \tan^{-1}(k_y/k_x)$ is the incident angle defined in momentum space. According to eq 7, the valley-resolved conductance can be introduced

$$G_{\mathrm{K}(\prime)} = \frac{G_{\mathrm{K}(\prime)\uparrow} + G_{\mathrm{K}(\prime)\downarrow}}{2} \quad (8)$$

and the valley- and spin-polarized conductance can be defined as[28]

$$G_v = \frac{G_{\mathrm{K}} - G_{\mathrm{K}'}}{G_{\mathrm{K}} + G_{\mathrm{K}'}} \quad (9)$$

$$G_s = \frac{G_{\mathrm{K}\uparrow} + G_{\mathrm{K}'\uparrow} - G_{\mathrm{K}'\downarrow} - G_{\mathrm{K}\downarrow}}{G_{\mathrm{K}\uparrow} + G_{\mathrm{K}'\uparrow} + G_{\mathrm{K}'\downarrow} + G_{\mathrm{K}\downarrow}} \quad (10)$$

In addition, the normalized charge conductance reads

dx.doi.org/10.1021/am4047602 | ACS Appl. Mater. Interfaces 2014, 6, 1759−1764

$$G_c = G_K + G_{K'} \quad (11)$$

RESULTS AND DISCUSSION

We note that the uppermost valence band (UVB) of ML MoS_2 at Γ point is quite close in energy to the K point. According to Ellis et al.,[11] the energy difference between the UVBs of Γ point and K point is $\delta E_{\Gamma-K} = 0.26$ eV. Considering that the effective continuum model described in eq 1 is only valid for the low-lying physics of ML MoS_2, we restrict the electrostatic potential U ranges from -0.3Δ to 2.2Δ in the following calculations and single out the exchange field $h = 0.2\Delta$ and the Fermi energy $E = 1.2\Delta$. In doing so, the largest energy separation between the UVB and the Fermi level at K point is $x_{max} = U_{max} + h - \Delta + 2\lambda - E \approx 0.24$ eV $< \delta E_{\Gamma-K}$, which means that the Fermi level, in all cases, can be immune to intersect with the valence bands near the Γ point. Therefore, for the transport properties addressed here, it is rational to neglect the contribution from the band near the Γ point, and the low-lying continuum model is appropriate for all calculations. In addition, it is reported that the lowermost of the conduction bands possess a spin splitting of about 3−4 meV.[20,22] Since it is one magnitude lower than the UVB spin splitting scale λ and two magnitudes lower than Δ, we neglect this spin splitting in this study.

We first investigate the valley-resolved conductance. Figure 2a illustrates the valley-resolved conductance $G_K(G_{K'})$ as a function of the normalized length $k_FL(k_F = E/(\hbar v))$. For $U = 0.2\Delta$, the valley-resolved conductances G_K and $G_{K'}$ take the same values, and both of them are insensitive to the length of the ferromagnetic MoS_2 strip L. Therefore, the valley-resolved transport is nonpolarized (see Figure 2b). When $U = 2.0\Delta$, G_K is totally suppressed while $G_{K'}$ takes finite value and oscillates with L. This phenomenon mainly originates from the opposite spin splitting of the valence-band edges near the K and K′ points. Moreover, the differences of the spin splitting between the two valleys can be further enlarged by the exchanged field h. Consequently, only the charge carriers stemming from the K′ valley can contribute to the conductance, which results in a *fully* valley-polarized transport, as shown in Figure 2b. When the normalized length k_FL is large enough (>7.6), the *fully* valley-polarized conductance can be achieved regardless of the ferromagnetic strip length L. For $k_FL < 7.6$, the valley-polarized conductance exponentially decays with decreasing the (normalized) sample length. These phenomena can be expected. For $U = 2.0\Delta$, the Fermi level drops into the energy gap of K valley (see Figure 5e), which results in the appearance of evanescent modes near the incident side of the ferromagnetic region. When the length L is small, these evanescent modes can also contribute to the transport by tunneling, which results in a finite K valley-resolved conductance. Therefore, the valley-polarized conductance exponentially decays with decreasing the sample length. As the tunneling probability exponentially decays with increasing L, the tunneling process is totally inhibited for a large L. Consequently, only the carriers near the K′ point can contribute to the transport when L is large enough, which results in a fully valley-polarized conductance regardless of the sample length. By passing, the critical value (L_c) of the sample length should be several the decay scales; here the decay scale can be defined as $1/|\mathrm{Im}(k_{x,\tau_z=1}')|$. In our calculation, the normalized critical scale k_FL_c is about 7.6.

Figure 2c,d exhibits the gate voltage U dependence of the valley-resolved and valley-polarized conductances, respectively. Red curves correspond to the conductance spectra when U/Δ ranges from −0.3 to −0.1, and blue curves denote the conductance spectra when U/Δ ranges from 1.9 to 2.2. As can be seen, both G_K and $G_{K'}$ oscillate with$U$ but take different values, so a finite valley-polarized conductance can be expected (see Figure 2d). Importantly, the differences between G_K and $G_{K'}$ vary with the gate voltage; this means the valley-polarized conductance can be effectively tuned by the gate voltage. When the gate voltage U ranges from 1.92Δ to 2.11Δ, a fully polarized conductance can be achieved. The Fermi level drops into the energy gap when U/Δ ranges from −0.1 to 1.9 and results in a trivial conductance $G = 0$, in which we omit the plots of this regime in Figure 2c,d.

Figure 3a presents the spin-polarized conductance as a function of the normalized sample length k_FL. For $U = 0.2\Delta$, since the spin degeneracy of the conduction band edges can be removed by the exchange field, a *fully* spin-polarized conductance is achieved. It is also observed that the spin-resolved conductance is *fully* polarized when $U = 2\Delta$, and this characteristic mainly results from the spin splitting on the top of the valence bands. We note that, for $U = 0.2\Delta$ and $U = 2\Delta$, the configurations of spin-polarized conductance spectra are similar to that of valley-polarized conductance spectra. This point can be understood by the similar mechanism that was mentioned in the valley-polarized transport. Because the Fermi level only intersects with spin up (down) bands for $U = 0.2\Delta$ ($U = 2\Delta$), evanescent modes can exist in the ferromagnetic

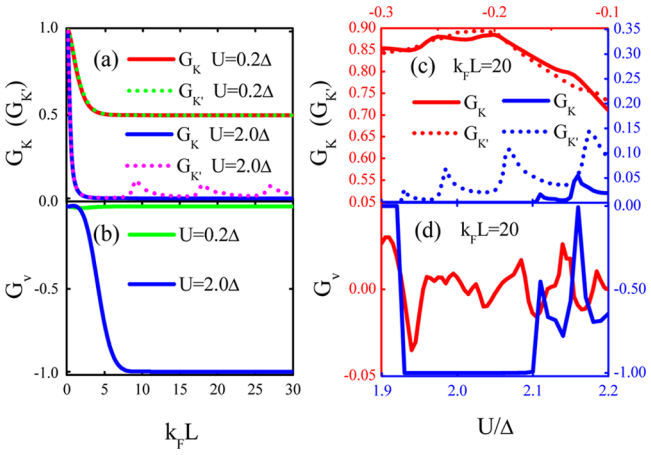

Figure 2. Dependence of k_FL (a) valley-resolved conductance $G_K(G_{K'})$ and (b) valley-polarized conductance. Gate voltage U dependence of (c) the resolved conductance $G_K(G_{K'})$ and (d) valley-polarized conductance; $h = 0.2\Delta$ and $E = 1.2\Delta$ in all panels.

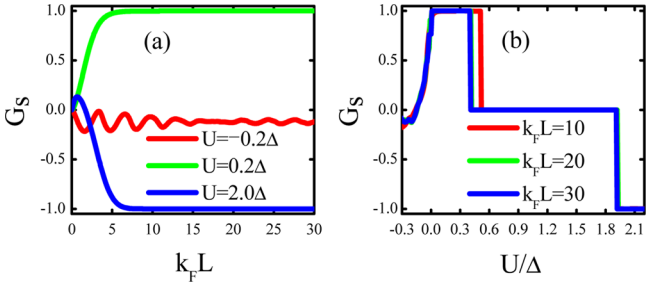

Figure 3. Spin-polarized conductance G_s as a function of L (a) and U (b); the other parameters are the same as those in Figure 2.

dx.doi.org/10.1021/am4047602 | ACS Appl. Mater. Interfaces 2014, 6, 1759−1764

region and contribute to the conductance when L is small enough. Here, the critical normalized length $k_F L_c \approx 7$. For the case of $U = -0.2\Delta$, the spin-polarized conductance exhibits slight oscillations but with nearly zero average values. It is observed that the exponential decaying characteristic disappears. Because the Fermi level, in this situation, simultaneously intersects with the spin up and down bands, evanescent modes cannot be induced. Consequently, the transport all originates from propagating modes, and the spin-polarized conductance exhibits nearly periodic oscillations. Figure 3b plots the spin-polarized conductance as a function of the gate voltage. As can be seen, both the amplitude and direction of the spin-polarized conductance can be effectively tuned by the gate voltage regardless of the sample length L, and the direction of the spin-polarized conductance can be controlled only by the gate voltage but without changing the direction of the exchange field.

The charge transport properties are shown in Figure 4. Owing to the tunneling effect, when $k_F L < 5$, the charge

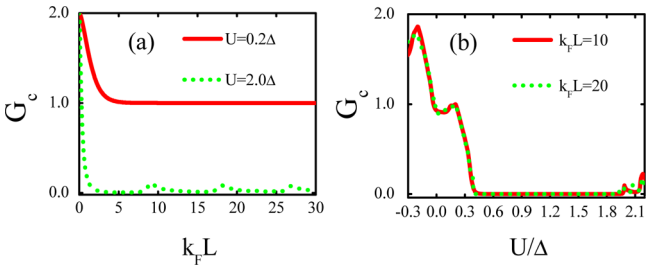

Figure 4. Normalized charge conductance G_c as a function of L (a) and U (b); the other parameters are the same as those in Figure 2.

conductance exponentially decreases with increasing $k_F L$. When $k_F L$ is greater than 5, the charge conductance exhibits quite different behaviors for small ($U = 0.2\Delta$) and large gate voltage ($U = 2\Delta$). This is because the transport processes in the two situations are different; namely, the intraband transport occurs for $U = 0.2\Delta$ while interband transport process occurs for $U = 2\Delta$. Because of the electron−hole asymmetry, the conductance of the interband transport process exhibits relatively large oscillations. Due to the relatively large energy gap, the charge conductance possesses a good on/off switching effect, which may be interesting for device application.

These interesting scenarios can be understood from the electronic structures in each region of the NFN junction, as shown in Figure 5. The left and right panels correspond to the K and K′ valleys, respectively. For normal regions (Figure 5a,b), the uppermost valence bands of two valleys possess opposite spin splitting. In the presence of exchange field (Figure 5c−h), the spin degeneracy on the bottom of the conduction bands is removed. Importantly, the exchange field can further extend the difference between the spin splitting gaps at the two valleys, this point is essential to the valley-polarized transport. For $U = 0.2\Delta$ (Figure 5c,d), the Fermi level crosses bands at both K and K′ valleys, so the charge carriers at both valleys can contribute to the conductance and result in a relatively large charge conductance but a nearly vanished valley-polarized conductance. On the other hand, a *fully* spin-polarized conductance can be achieved because the Fermi level only intersects with the spin up bands. When $U = 2\Delta$, as illustrated in Figure 5e,f, the Fermi level only crosses the spin down band of the K′ valley due to the spin splitting together

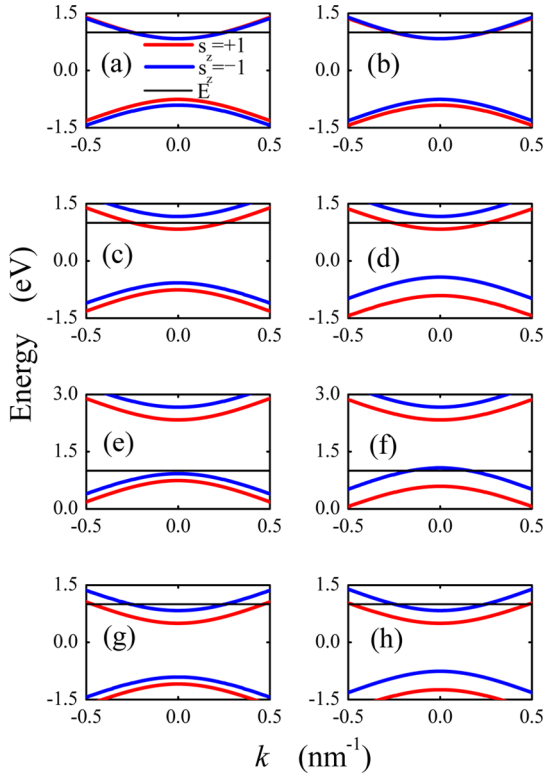

Figure 5. Band structures at the K and K′ valleys. The left (right) panel denotes the K(K′) valley. Red ($s_z = +1$) and blue ($s_z = -1$) curves correspond to the spin up and down bands, respectively. The other parameters are taken as follows: (a,b) $h = 0$ and $U = 0$; (c,d) $h = 0.2\Delta$ and $U = 0.2\Delta$; (e,f) $h = 0.2\Delta$ and $U = 2.0\Delta$; (g,h) $h = 0.2\Delta$ and $U = -0.2\Delta$. Black horizontal lines in all panels denote the Fermi levels $E = 1.2\Delta$.

with the exchange field. Therefore, only the spin down charge carriers stemming from the K′ valley can contribute to the conductance, and both *full* valley- and spin-polarized conductance can be achieved in this situation. We emphasize here that this scenario originates from the spin splitting on the top of the valence bands, which is quite different from that of graphene[26,27] and silicene.[28] The case of $U = -0.2\Delta$ is shown in Figure 5g,h. As can be seen, the Fermi level crosses both the spin up and down bands, and thus the charge carriers with spin up and down at both valleys can equally contribute to the conductance. Consequently, both the valley and spin transport are not polarized.

From the above discussion, it is concluded that one valley should be totally suppressed while the other must keep conductive to realize the full valley-polarized transport. To do so, the gate voltage U and the exchange field h should satisfy the quantitative condition

$$|2\lambda - |h|| < E - U + \Delta < 2\lambda + |h| \quad (12)$$

For the *fully* spin-polarized transport, the Fermi level should only intersect with spin up (down) bands at both valleys, and the quantitative condition is given by

$$|E - U + \Delta - 2\lambda| < |h| \quad (13)$$

Owing to the exchange field, the Fermi level can also be tuned to the bottom of the conduction bands to realize the *fully* spin-polarized transport, and the condition reads

$$|E - U - \Delta| < |h| \quad (14)$$

dx.doi.org/10.1021/am4047602 | ACS Appl. Mater. Interfaces 2014, 6, 1759−1764

These conditions are illustrated in Figure 6, where we present the contour plots of (a) valley- and (b) spin-polarized

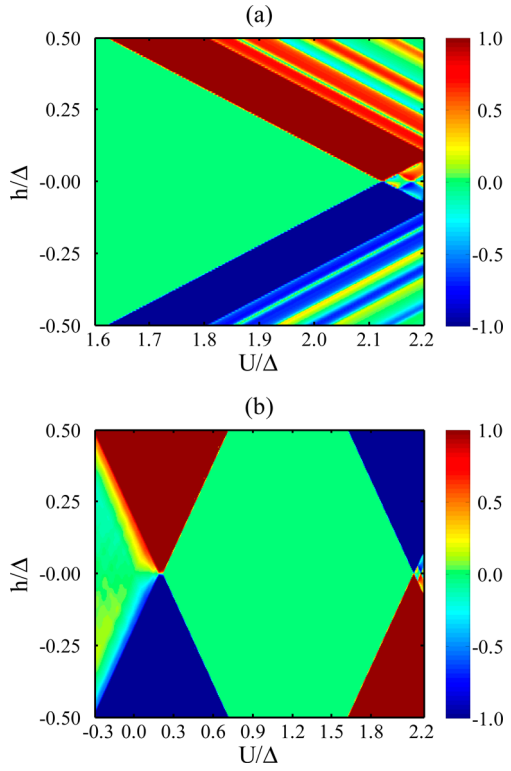

Figure 6. Contour plots of (a) valley polarization conductance G_v (b) and spin polarization conductance G_s as functions of h and U with k_FL = 20 and E = 1.2Δ.

conductance, with k_FL = 20 and E = 1.2Δ. As can be seen, both the valley- and spin-polarized conductances are odd functions of h; this means that the polarization directions are associated with the exchange field. It is observed that the spin-polarized conductance can be realized within a large range of gate voltage. More importantly, both the amplitude and direction of spin-polarized conductance can be modulated by the gate voltage.

In this work, the band overlapping is not considered, so the exchange field should satisfy

$$|h| < (\Delta - \lambda) \tag{15}$$

The electrically controllable valley- and spin-polarized transport properties in the present work are based on the novel spin and valley physics of ML MoS_2. To practically realize these properties, the sample length should be large enough to suppress the tunneling effect, and the exchange field can be induced by the magnetic proximity effect caused by magnetic insulators.

CONCLUSION

In conclusion, the charge, valley, and spin transport properties of a NFN MoS_2 junction have been carefully studied. It was found that the charge, valley, and spin transport in this junction can be effectively manipulated by a gate voltage. Owing to the spin−valley coupling of valence-band edges, the *fully* spin- and valley-polarized conductances can be simultaneously obtained. Moreover, both the amplitude and direction of the spin-polarized conductance can be conveniently controlled by the gate voltage. It was observed that the charge transport in the proposed device is insensitive to the structure parameters, which is a benefit for the device manufacture. The band structures in each region of the NFN MoS_2 junction were introduced to understand these novel transport results. The conditions for realizing the *fully* valley- and spin-polarized conductance are analytically concluded. These results provide an avenue for the electrical control of valley- and spin-polarized transport in MoS_2-based devices.

AUTHOR INFORMATION

Corresponding Author

*E-mail: stsygw@mail.sysu.edu.cn.

Notes

The authors declare no competing financial interest.

ACKNOWLEDGMENTS

This work is supported by the State Key Laboratory of Optoelectronic Materials and Technologies of Sun Yat-sen University. D.X.Y. is supported by NBRPC-2012CB821400, NCET-11-0547, and RFDPHE-20110171110026.

REFERENCES

(1) Novoselov, K. S.; Geim, A. K.; Morozov, S. V.; Jiang, D.; Zhang, Y.; Dubonos, S. V.; Grigorieva, I. V.; Firsov, A. A. *Science* **2004**, *306*, 666−669.
(2) Novoselov, K. S.; Geim, A. K.; Morozov, S. V.; Jiang, D.; Katsnelson, M. I.; Grigorieva, I. V.; Dubonos, S. V.; Firsov, A. A. *Nature* **2005**, *438*, 197−200.
(3) Novoselov, K. S.; Jiang, D.; Schedin, F.; Booth, T. J.; Khotkevich, V. V.; Morozov, S. V.; Geim, A. K. *Proc. Natl. Acad. Sci. U.S.A.* **2005**, *102*, 10451−10453.
(4) Liu, C.-C.; Feng, W.; Yao, Y. *Phys. Rev. Lett.* **2011**, *107*, 076802.
(5) Chen, L.; Liu, C.-C.; Feng, B.; He, X.; Cheng, P.; Ding, Z.; Meng, Z.; Yao, Y.; Wu, K. *Phys. Rev. Lett.* **2012**, *109*, 056804.
(6) Mak, K. F.; Lee, C.; Hone, J.; Shan, J.; Heinz, T. F. *Phys. Rev. Lett.* **2010**, *105*, 136805.
(7) Xiao, D.; Liu, G.-B.; Feng, W.; Xu, X.; Yao, W. *Phys. Rev. Lett.* **2012**, *108*, 196802.
(8) Lu, H.-Z.; Yao, W.; Xiao, D.; Shen, S.-Q. *Phys. Rev. Lett.* **2013**, *110*, 016806.
(9) Li, X.; Zhang, F.; Niu, Q. *Phys. Rev. Lett.* **2013**, *110*, 066803.
(10) Splendiani, A.; Sun, L.; Zhang, Y.; Li, T.; Kim, J.; Chim, C.-Y.; Galli, G.; Wang, F. *Nano Lett.* **2010**, *10*, 1271−1275.
(11) Ellis, J. K.; Lucero, M. J.; Scuseria, G. E. *Appl. Phys. Lett.* **2011**, *99*, 261908.
(12) Lee, H. S.; Min, S.-W.; Chang, Y.-G.; Park, M. K.; Nam, T.; Kim, H.; Kim, J. H.; Ryu, S.; Im, S. *Nano Lett.* **2012**, *12*, 3695−3700.
(13) Cappelluti, E.; Roldán, R.; Silva-Guillén, J. A.; Ordejón, P.; Guinea, F. *Phys. Rev. B* **2013**, *88*, 075409.
(14) Radisavljevic, B.; Radenovic, A.; Brivio, J.; Giacometti, V.; Kis, A. *Nat. Nanotechnol.* **2011**, *6*, 147−150.
(15) Wang, Q. H.; Kalantar-Zadeh, K.; Kis, A.; Coleman, J. N.; Strano, M. S. *Nat. Nanotechnol.* **2012**, *7*, 699−712.
(16) Liu, H.; Neal, A. T.; Ye, P. D. *ACS Nano* **2012**, *6*, 8563−8569.
(17) Yoon, Y.; Ganapathi, K.; Salahudin, S. *Nano Lett.* **2011**, *11*, 3768−3773.
(18) Neto, A. H. C.; Guinea, F.; Peres, N. M. R.; Novoselov, K. S.; Geim, A. K. *Rev. Mod. Phys.* **2009**, *81*, 109−162.
(19) Sarma, S. D.; Adam, S.; Hwang, E. H.; Rossi, E. *Rev. Mod. Phys.* **2011**, *83*, 407−470.
(20) Cheiwchanchamnangij, T.; Lambrecht, W. R. L. *Phys. Rev. B* **2012**, *85*, 205302.
(21) Zhu, Z. Y.; Cheng, Y. C.; Schwingenschlögl, U. *Phys. Rev. B* **2011**, *84*, 153402.

(22) Kormányos, A.; Zólymi, V.; Drummond, N. D.; Rakyta, P.; Burkard, G.; Fal'ko, V. I. *Phys. Rev. B* **2013**, *88*, 045416.
(23) Mak, K. F.; He, K.; Shan, J.; Heinz, T. F. *Nat. Nanotechnol.* **2012**, *7*, 494−498.
(24) Cao, T.; Wang, G.; Han, W.; Ye, H.; Zhu, C.; Shi, J.; Niu, Q.; Tan, P.; Wang, E.; Liu, B.; Feng, J. *Nat. Commun.* **2012**, *3*, 887.
(25) Zeng, H.; Dai, J.; Yao, W.; Xiao, D.; Cui, X. *Nat. Nanotechnol.* **2012**, *7*, 490−493.
(26) Yokoyama, T. *Phys. Rev. B* **2008**, *77*, 073413.
(27) Haugen, H.; Huertas-Hernando, D.; Brataas, A. *Phys. Rev. B* **2008**, *77*, 115406.
(28) Yokoyama, T. *Phys. Rev. B* **2013**, *87*, 241409(R).
(29) Ramasubramaniam, A.; Naveh, D.; Towe, E. *Phys. Rev. B* **2011**, *84*, 205325.
(30) Dolui, K.; Pemmaraju, D. C.; Sanvito, S. *ACS Nano* **2012**, *6*, 4823−4834.
(31) Qi, J.; Li, X.; Qian, X.; Feng, J. *Appl. Phys. Lett.* **2013**, *102*, 173112.
(32) Ye, P. D.; Weiss, D.; Gerhards, R. R.; Seeger, M.; von Klitzing, K.; Eberl, K.; Nickel, H. *Phys. Rev. Lett.* **1995**, *74*, 3013.
(33) Bai, C.; Zhang, X. *Phys. Rev. B* **2007**, *76*, 075430.
(34) Barbier, M.; Vasilopoulos, P.; Peeters, F. M. *Phys. Rev. B* **2009**, *80*, 205415.
(35) Wang, L.-G.; Zhu, S.-Y. *Phys. Rev. B* **2010**, *81*, 205444.
(36) Mondal, S.; Sen, D.; Sengupta, K.; Shankar, R. *Phys. Rev. Lett.* **2010**, *104*, 046403.
(37) Yamakage, A.; Imura, K.-I.; Cayssol, J.; Kuramoto, Y. *Phys. Rev. B* **2011**, *83*, 125401.
(38) Yokoyama, T.; Tanaka, Y.; Nagaosa, N. *Phys. Rev. B* **2010**, *81*, 121401.